IOP Publishing Journal of Physics G: Nuclear and Particle Physics
J. Phys. G: Nucl. Part. Phys. **47** (2020) 035102 (15pp) https://doi.org/10.1088/1361-6471/ab5400

Nuclear matrix elements of neutrinoless double beta decay for masses 130 and 136 in the shell model

K Higashiyama[1], K Yanase[2], N Yoshinaga[3], A Umeya[4], A Uehara[3] and E Teruya[3]

[1] Department of Physics, Chiba Institute of Technology, Narashino, Chiba 275-0023, Japan
[2] Center for Nuclear Study, University of Tokyo, Hongo, Bunkyo-ku, Tokyo 113-0033, Japan
[3] Department of Physics, Saitama University, Saitama City 338-8570, Japan
[4] Liberal Arts and Sciences, Nippon Institute of Technology, Miyashiro, Saitama 345-8501, Japan

E-mail: koji.higashiyama@it-chiba.ac.jp

Received 15 August 2019, revised 30 October 2019
Accepted for publication 4 November 2019
Published 22 January 2020

Abstract

The nuclear matrix elements (NMEs) for the $0\nu\beta\beta$ decays from ^{130}Te to ^{130}Xe and from ^{136}Xe to ^{136}Ba are calculated in the nuclear shell model. In order to investigate the model dependence on the NMEs, pair-truncated shell-model calculations are also performed. It is found that the NMEs are sensitive to the ground-state correlations. In particular, the isovector monopole-pairing interactions largely affect the NMEs.

Keywords: shell model, collective levels, neutrinoless double beta decay

(Some figures may appear in colour only in the online journal)

1. Introduction

For nuclei of mass number $A \sim 130$, various characteristic phenomena in the nuclear structure are known. One is the appearance of the doublet bands in doubly-odd nuclei, which are almost energetically degenerate $\Delta I = 1$ bands with the same parity [1–3]. The doublet bands are theoretically analyzed in terms of the phenomenological particle-rotor model [4], the projected shell model [5, 6], the quadrupole coupling model [7–10], and the pair-truncated shell model (PTSM) [11–14]. Moreover, isomers signaling the change of nuclear structure are present in this mass region. For example, isomers with spin-parity 10^+ are systematically present in even–even Sn isotopes [15]. Recently, new isomeric states have been found in ^{135}La

[16] and ^{136}La [17], but the nature of those isomers still needs to be unveiled. These isomeric states in this mass region were systematically analyzed in the nuclear shell model (SM) [18, 19].

Double beta decay is the process in which two successive β decays occur inside a nucleus (see e.g. [20, 21] for reviews). This second-order process of the weak interaction can take place through the 2ν mode ($2\nu\beta\beta$) within the Glashow–Weinberg–Salam theory of electroweak interactions. The $2\nu\beta\beta$ decay is characterized by the emission of two electrons and two electron anti-neutrinos. The half-lives in the $2\nu\beta\beta$ decay have been experimentally observed in ten nuclei so far [22]. Many theoretical attempts have been made to calculate the nuclear matrix elements (NMEs) and their half-lives [23–27].

In contrast the 0ν mode ($0\nu\beta\beta$) occurs when the first emitted electron anti-neutrino is absorbed by another neutron as an electron neutrino. This process can take place only if the electron neutrino is a Majorana particle and the helicity matching is satisfied. The observation of the $0\nu\beta\beta$ decay demands an extension of the Standard Model of particle physics since it violates the lepton number conservation. Thus, the $0\nu\beta\beta$ decay is considered as one of the best probes for physics beyond the Standard Model. Despite intensive experimental efforts (see e.g. [28] for a review), the $0\nu\beta\beta$ decay has not been observed yet.

The NMEs for the $0\nu\beta\beta$ decays have been calculated in several nuclear models such as the SM [29–39], the quasi-particle random-phase approximation (QRPA) [23, 40–50], the interacting boson model (IBM) [51–54], and energy density function (EDF) theory including EDF-based generator coordinate method (GCM) calculations [55–60]. However, there still remain large differences in the NMEs calculated in these models. In order to clarify the disagreements, it is important to obtain the precise nuclear wavefunctions that reproduce not only the experimental energy levels, but also the electromagnetic properties of the nuclei concerned.

In the previous paper [39], SM calculations were carried out for isobaric nuclei with mass numbers 76 and 82. The NMEs of the $0\nu\beta\beta$ decays of ^{76}Ge and ^{82}Se are calculated with the use of the wavefunctions obtained in the SM. It was found in comparison to the results in the PTSM that the NMEs are sensitive to the pairing gaps in the ground states, namely, sensitive to the ground state correlations.

In this paper we focus on the $0\nu\beta\beta$ decay from ^{130}Te to ^{130}Xe, and that from ^{136}Xe to ^{136}Ba. Recently, experimental results of ^{136}Xe have been presented [61, 62], which give a lower limit on the half-life of 1.07×10^{26} yr. Also for the $0\nu\beta\beta$ decay of ^{130}Te, a lower limit of 1.5×10^{25} yr has been reported [63]. In the first part of this paper, SM calculations are performed for the ^{130}Te, ^{130}Xe, ^{136}Xe, and ^{136}Ba nuclei. An extended pairing plus quadrupole interaction is employed as a shell-model effective interaction, and the one-major single-particle orbitals between magic numbers 50 and 82 are taken into account. In the second part, the NME of the $0\nu\beta\beta$ decay is calculated for the transition from the ground state of ^{130}Te (^{136}Xe) to that of ^{130}Xe (^{136}Ba). In addition to the SM, the PTSM is employed to construct the wavefunctions of the nuclei, and then to calculate the NMEs. The PTSM is helpful to analyze the correlations between the NMEs and nuclear structure. In particular, the sensitivity to the numbers of S pairs in the ground states is demonstrated. The NMEs obtained in the SM and in the PTSM are compared with those in other studies. In order to investigate the correlations of the NMEs with other physical quantities, the occupation numbers are calculated. Moreover, the sensitivity of the NMEs to the isovector monopole-pairing strengths is investigated.

This paper is organized as follows. Section 2 provides the frameworks of the present SM and PTSM calculations. The energy spectra in the SM and the PTSM are compared with the experimental data. In section 3 the NMEs of the $0\nu\beta\beta$ decays in the SM and the PTSM are

given and compared with those in other models. Discussions are given in section 4. Finally, the present work is summarized in section 5.

2. Shell-model calculations for nuclear structure

In the present paper, ^{130}Te, ^{130}Xe, ^{136}Xe, and ^{136}Ba nuclei are studied in the nuclear shell model (SM). For single-particle orbitals, all the five orbitals in the one major-shell between magic numbers 50 and 82, namely, $1d_{3/2}$, $0h_{11/2}$, $2s_{1/2}$, $1d_{5/2}$, and $0g_{7/2}$ orbitals, are taken into account for both neutrons and protons. The single-particle energies ϵ_τ ($\tau = \nu$ or π) are the same as a previous study [18].

As a nuclear effective interaction, an extended pairing plus quadrupole interaction is employed. The SM Hamiltonian is written as

$$H = H_\nu + H_\pi + H_{\nu\pi}, \tag{1}$$

where H_ν, H_π, and $H_{\nu\pi}$ represent the neutron interaction, the proton interaction, and the neutron–proton interaction, respectively. The Hamiltonian among like nucleons H_τ ($\tau = \nu$ or π) consists of the single-particle energies, monopole-pairing (MP) interactions, quadrupole–quadrupole (QQ) interactions, and higher multipole-pairing interactions, i.e.

$$\begin{aligned} H_\tau = & \sum_{jm} \epsilon_{j\tau} c^\dagger_{jm\tau} c_{jm\tau} - G_{0\tau} P^{\dagger(0)}_\tau P^{(0)}_\tau - \kappa_\tau : Q_\tau \cdot Q_\tau : \\ & - \sum_{L=2,4,6,8,10} G_{L\tau} P^{\dagger(L)}_\tau \cdot \tilde{P}^{(L)}_\tau, \end{aligned} \tag{2}$$

where : : denotes the normal ordering. It is assumed that the interaction between neutrons and protons $H_{\nu\pi}$ is just given by the QQ interaction as

$$H_{\nu\pi} = -\kappa_{\nu\pi} Q_\nu \cdot Q_\pi. \tag{3}$$

The adopted two-body interaction strengths are given in table 2 of [18]. The MP strengths for neutrons and protons are given as $G_{0\nu} = 0.170$ MeV and $G_{0\pi} = 0.165$ MeV, respectively. The SM results reproduced using the above $G_{0\tau}$ values are referred to as the optimized shell model results hereafter. These values were determined to optimize the experimental energy spectra of 46 nuclei in the mass number $A \sim 130$ region [18].

Low-lying energy levels in the SM are shown on the middle left panel in figure 1, which are compared with the experimental data on the far left panel. The energy levels of the yrast states are well reproduced in the SM. In particular, there is a large energy gap between the 6^+_1 and 8^+_1 states, whereas the gap between the 4^+_1 and 6^+_1 states is small. This experimental situation is well reproduced. This arises from the fact that two protons occupying the $0g_{7/2}$ orbital can be coupled with spins up to 6.

In order to examine how the MP strengths affect the energy spectra, we artificially make the isovector monopole strengths $G_{0\tau}$ ($\tau = \nu$, π) larger as

$$G'_{0\tau} = x\, G_{0\tau} \tag{4}$$

by changing the parameter x ($1 \leqslant x \leqslant 2$). The strengths of other interactions are kept intact. On the middle right panel in figure 1, the energy spectrum with $x = 1.3$ is shown. In this case the excitation energy of the 2^+_1 state is 1.65 times larger than that using the optimized MP strengths.

In the PTSM [11–14], the full SM space is restricted within a subspace where collective pairs with angular momenta of zero (S pair), two (D pair), and four (G pair) and non-collective pairs associated with the $0h_{11/2}$ orbital (H pair) are used as building blocks. The

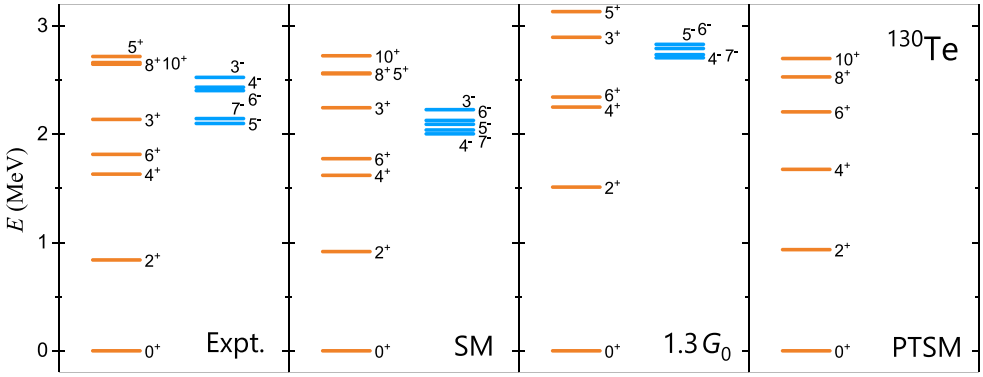

Figure 1. Comparison between the low-lying energy levels of ^{130}Te in experiment (Expt.) and those in the present shell model (SM). The SM results using the MP strength 1.3 times larger than the optimized value ($1.3G_0$) and the PTSM results (PTSM) are also shown. Experimental data are taken from [64, 65].

collective S, D, and G pairs are defined as

$$S^\dagger = \sum_j \alpha_j A_0^{\dagger(0)}(jj), \tag{5}$$

$$D_M^\dagger = \sum_{j_1 j_2} \beta_{j_1 j_2} A_M^{\dagger(2)}(j_1 j_2), \tag{6}$$

$$G_M^\dagger = \sum_{j_1 j_2} \gamma_{j_1 j_2} A_M^{\dagger(4)}(j_1 j_2), \tag{7}$$

where $A_M^{\dagger(J)}(j_1 j_2)$ is the nucleon-pair creation operator defined by

$$A_M^{\dagger(J)}(j_1 j_2) = \sum_{m_1 m_2} (j_1 m_1 j_2 m_2 |\, JM) c_{j_1 m_1}^\dagger c_{j_2 m_2}^\dagger = [c_{j_1}^\dagger c_{j_2}^\dagger]_M^{(J)}, \tag{8}$$

where $(j_1 m_1 j_2 m_2 |\, JM)$ stands for the Clebsch–Gordan coefficients. The non-collective H pairs are defined with the creation operator of

$$H_M^{\dagger(K)} = [c_{11/2}^\dagger\, c_{11/2}^\dagger]_M^{(K)}, \tag{9}$$

where $K = 0$, 2, 4, 6, 8, and 10. In contrast to the S, D, and G pairs, the H pairs are non-collective, since they have unique structure consisting of two nucleons in the $0h_{11/2}$ orbital.

A many-body configuration is constructed by applying the above operators on the closed-shell core $|-\rangle$ as

$$|S^{n_s} D^{n_d} G^{n_g} H^{n_h} \eta I\rangle = (S^\dagger)^{n_s} (D^\dagger)^{n_d} (G^\dagger)^{n_g} (H^\dagger)^{n_h} |-\rangle, \tag{10}$$

where n_s, n_d, n_g, and n_h represent the numbers of S, D, G, and H pairs, respectively. Here, I represents the nuclear spin and η represents other quantum numbers to identify many-body states. The coupling of angular momentum is completely carried out, but for simplicity the coupling is not explicitly denoted. The Hamiltonian with the same set of the single-particle energies and the interaction strengths as the SM calculations is diagonalized in the PTSM subspace. On the far right panel in figure 1, the spectrum of ^{130}Te in the PTSM is shown. The position of the 2_1^+ state is almost reproduced, but the small energy gap between the 4_1^+ state

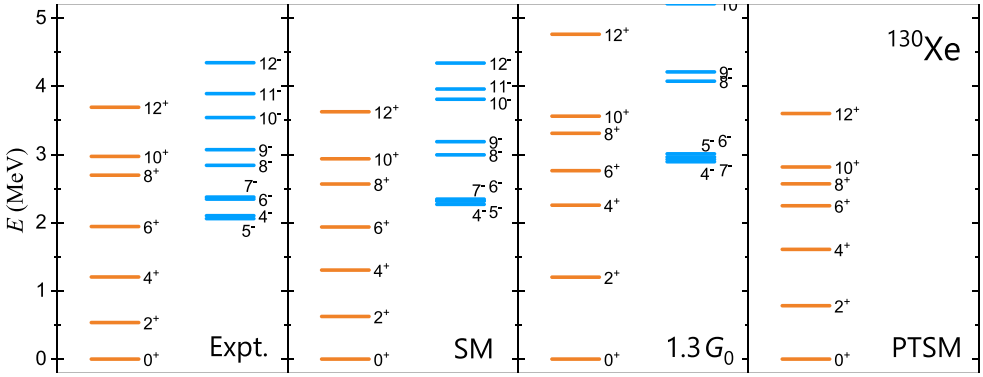

Figure 2. Same as figure 1, but for ^{130}Xe. Experimental data are taken from [64].

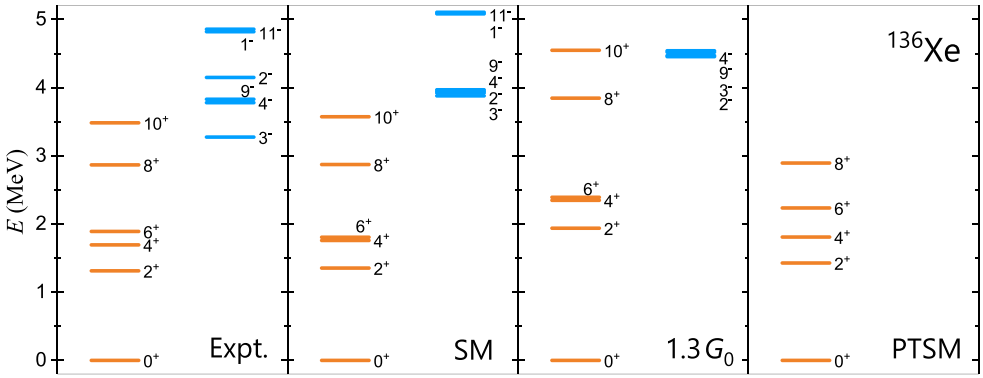

Figure 3. Same as figure 1, but for ^{136}Xe. Experimental data are taken from [66].

and the 6_1^+ state is not reproduced well. The negative parity states are out of the present PTSM framework because the parity of all the pairs is positive.

The energy spectra of ^{130}Xe are shown in figure 2. The experimental level spacing between the 8_1^+ state and the 10_1^+ state is small, whereas there is a large energy gap between the 10_1^+ state and the 12_1^+ state. The SM calculation well reproduces these features in the yrast band. In the SM with $x = 1.3$ ($1.3G_0$), the excitation energy of the 2_1^+ state is high and the spacing between the 10_1^+ state and the 12_1^+ state is wide in comparison to experiment. On the other hand, the PTSM fairly reproduces the experimental energy spectrum. The energy spectra of ^{136}Xe are shown in figure 3. The ^{136}Xe nucleus is single-closed with four valence protons. The 6_1^+ state is an isomer with a half-life of 2.95(9) μs. The SM reproduces not only the small energy spacing between the 4_1^+ state and the 6_1^+ state, but also the small $B(E2; 6_1^+ \rightarrow 4_1^+)$ value [18]. The energy spectra of ^{136}Ba are shown in figure 4. In the SM the low-lying positive parity states with spins up to 6 are well reproduced, but the spacing between the 8_1^+ state and the 10_1^+ state is small. In the case of the SM with 1.3 G_0, energy gaps between the ground state and the 2_1^+ state and between the 2_1^+ and the 4_1^+ states are large.

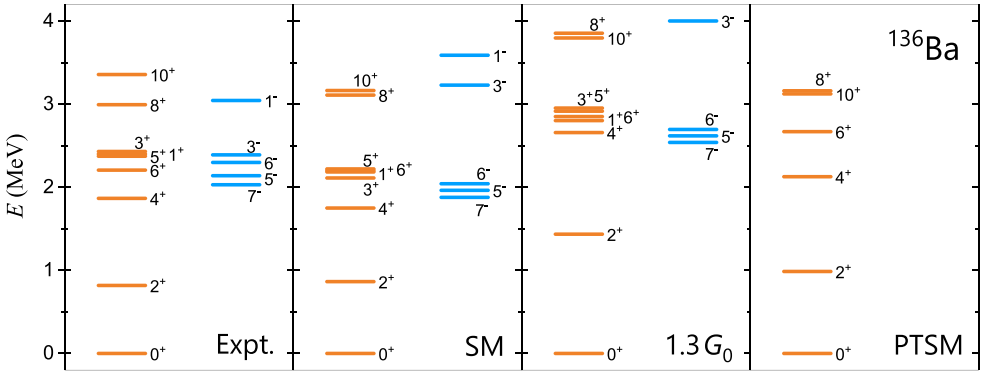

Figure 4. Same as figure 1, but for ^{136}Ba. Experimental data are taken from [66].

Table 1. The adopted parameters for each type, Fermi (F), Gamow–Teller (GT), and tensor (T).

K	F	GT	T
λ	0	0	2
s_1	0	1	1
s_2	0	1	1
$A^{(\lambda)}_{s_1 s_2}$	1	$-\sqrt{3}$	$\sqrt{2/3}$

3. Theoretical framework and results for neutrinoless double beta decay

The inverse of the half-life of the $0\nu\beta\beta$ decay is given as [20, 67]

$$[T^{(0\nu)}_{1/2}]^{-1} = G^{(0\nu)}(g_A)^4 |M^{(0\nu)}|^2 \left(\frac{\langle m_\nu \rangle}{m_e}\right)^2, \tag{11}$$

where $G^{(0\nu)}$ is the phase-space factor [68, 69], g_A the axial coupling constant, $\langle m_\nu \rangle$ the effective mass of the electron neutrino, m_e the electron mass, and $M^{(0\nu)}$ the NME.

The NME of the $0\nu\beta\beta$ decay can be written as

$$M^{(0\nu)} = \sum_K M^{(0\nu)}_K = M^{(0\nu)}_{\rm F} + M^{(0\nu)}_{\rm GT} + M^{(0\nu)}_{\rm T}, \tag{12}$$

where K indicates either Fermi (F), Gamow–Teller (GT), or tensor (T) type. Note that we do not follow the usual definition of the Fermi-type NME. The NME of each type is given by the corresponding neutrino potential $\hat{V}_K$ as [40]

$$M^{(0\nu)}_K = \langle \Psi_{\rm fin}(0^+_{\rm g.s.})|\ \hat{V}_K |\Psi_{\rm ini}(0^+_{\rm g.s.})\rangle, \tag{13}$$

where $|\Psi_{\rm ini}(0^+_{\rm g.s.})\rangle$ and $|\Psi_{\rm fin}(0^+_{\rm g.s.})\rangle$ stand for the wavefunctions of the ground states in the initial (parent) and final (daughter) nuclei, respectively. The neutrino potentials are given as [51]

$$\hat{V}_K = A^{(\lambda)}_{s_1 s_2} \sqrt{\frac{\pi}{2\lambda+1}} \sum_{ij} \tau^+_i \tau^+_j H_{\lambda,K}(r_{ij}) \times (Y^{(\lambda)}(\theta_{ij}, \varphi_{ij}) \cdot [\Sigma^{(s_1)}_i \otimes \Sigma^{(s_2)}_j]^{(\lambda)}), \tag{14}$$

where i or j represents each nucleon in a nucleus. Here, $\Sigma^{(s)} = 1$ for $s = 0$ and $\Sigma^{(s)} = \boldsymbol{\sigma}$ for $s = 1$. The τ^+ is the isospin raising operator and the $Y^{(\lambda)}$ indicates the spherical harmonics of

Table 2. NMEs in dimensionless units for the $0\nu\beta\beta$ decay from ^{130}Te to ^{130}Xe are shown. Our results in the shell-model are denoted as SM (optimized) and those with the monopole-pairing strengths which are 1.3 times stronger than the original ones are denoted as SM ($1.3G_0$). For the PTSM calculations, the results within the *SDGH* subspace, those within the *SDG* subspace, and those within the *SD* subspace are presented. They are compared with other works in several nuclear models, the SM [31, 35], the GCM [60], the QRPA [47], and the IBM [54]. The axial coupling constant g_A adopted in each study is given in the second column. In the last column half-lives are given in units of 10^{30} yr $\cdot$ meV^2, where the phase-space factor is taken from [68] except for the SM (GCN50.82) [31].

Model (Interaction)	g_A	$M_{\rm F}^{(0\nu)}$	$\widetilde{M}_{\rm F}^{(0\nu)}$	$M_{\rm GT}^{(0\nu)}$	$M_{\rm T}^{(0\nu)}$	$M^{(0\nu)}$	$T_{1/2}^{(0\nu)}\langle m_\nu\rangle^2$
SM (optimized)	1.25	0.567	−0.886	0.720	−0.186	1.101	6.18
SM ($1.3G_0$)	1.25	0.929	−1.451	1.325	−0.268	1.986	1.90
PTSM-*SDGH*	1.25	0.845	−1.320	1.276	−0.243	1.877	2.13
PTSM-*SDG*	1.25	0.919	−1.436	1.558	−0.249	2.227	1.51
PTSM-*SD*	1.25	1.016	−1.588	1.876	−0.261	2.631	1.08
SM (SVD) [35]	1.254		−0.44	1.66	−0.01	1.94	
SM (GCN50.82) [31]	1.25					2.12	1.29
GCM [60]	1.254		−0.47	2.25	−0.02	2.52	
QRPA (Argonne V18) [47]	1.27		−1.546	3.478	−0.550	3.888	
QRPA (CD-Bonn) [47]	1.27		−1.637	3.852	−0.496	4.373	
IBM [54]	1.269		−0.65	3.43	−0.13	3.70	0.52

rank λ. The adopted coefficient $A_{s_1s_2}^{(\lambda)}$ of each type (F, GT, or T) is given in table 1 together with the parameters λ, s_1, and s_2.

The orbital part of the neutrino potential for each K, $H_{\lambda,K}(r_{ij})$, is explicitly given in the momentum representation as

$$H_{\lambda,K}(r) = \frac{2R}{(g_A)^2}\int \frac{2}{\pi}\frac{1}{q(q+\tilde{A})}h^K(q)j_\lambda(qr)q^2{\rm d}q, \tag{15}$$

where j_λ is the spherical Bessel function of rank λ, and R the nuclear radius $R = 1.2A^{1/3}$ (fm) for a mass number A. The explicit forms of $h^K(q)$ are given in appendix of [39]. The short-range correlation is taken into account by multiplying the orbital part of the each type neutrino potential by the Jastrow function squared, $f(r)^2$, with $f(r) = 1 - {\rm e}^{-ar^2}(1 - br^2)$. In the present calculation the Miller-Spencer parametrization where $a = 1.1$ fm^{-2} and $b = 0.68$ fm^{-2} is adopted [70]. The explicit formula of calculating the NMEs and the method of incorporating the short-range correlation are given in appendix of [39]. In the following, the closure approximation is taken with the closure energies of $\tilde{A} = \langle E_N\rangle - (\langle E_I\rangle + \langle E_F\rangle)/2$. Here $\langle E_N\rangle$, $\langle E_I\rangle$, and $\langle E_F\rangle$ stand for the energies of the intermediate state, the initial state, and the final state, respectively. The closure energies $\tilde{A}$ are taken as 13.28 MeV and 13.1 MeV for mass numbers $A = 130$ and $A = 136$, respectively [23].

The NME of the $0\nu\beta\beta$ decay from ^{130}Te to ^{130}Xe is calculated in the SM using the wavefunctions obtained in the previous section. The result is shown in the first row denoted by SM (optimized) of table 2 and compared with other calculations in the SM [31, 35], the GCM [60], the quasi-particle random phase approximation (QRPA) [47], and the IBM [54]. It should be noted that our definition of the Fermi-type NME, $M_{\rm F}^{(0\nu)}$ in equation (12), is different from other literatures. The conventionally defined Fermi-type NMEs, $\widetilde{M}_{\rm F}^{(0\nu)} = -[g_A/g_V]^2 M_{\rm F}^{(0\nu)}$ with $g_A = 1.25$ are also shown in table 2. The half-lives $T_{1/2}^{(0\nu)}$ multiplied by the effective neutrino

Table 3. Same as table 2, but for the $0\nu\beta\beta$ decay from ^{136}Xe to ^{136}Ba.

Model (Interaction)	g_A	$M_{\rm F}^{(0\nu)}$	$\widetilde{M}_{\rm F}^{(0\nu)}$	$M_{\rm GT}^{(0\nu)}$	$M_{\rm T}^{(0\nu)}$	$M^{(0\nu)}$	$T_{1/2}^{(0\nu)}\langle m_\nu\rangle^2$
SM (optimized)	1.25	0.478	−0.747	0.803	−0.135	1.145	5.57
SM ($1.3G_0$)	1.25	0.712	−1.113	1.235	−0.185	1.763	2.35
PTSM-*SDGH*	1.25	0.630	−0.984	0.932	−0.169	1.394	3.76
PTSM-*SDG*	1.25	0.626	−0.978	0.818	−0.177	1.267	4.55
PTSM-*SD*	1.25	0.715	−1.117	1.252	−0.180	1.787	2.29
SM (SVD) [35]	1.254		−0.40	1.50	−0.01	1.76	
SM (GCN50.82) [31]	1.25					1.76	1.78
GCM [60]	1.254		−0.32	2.17	−0.02	2.35	
QRPA (Argonne V18) [47]	1.27		−0.806	1.959	−0.282	2.177	
QRPA (CD-Bonn) [47]	1.27		−0.858	2.181	−0.254	2.460	
IBM [54]	1.269		−0.52	2.83	−0.10	3.05	0.74

mass squared $\langle m_\nu\rangle^2$, which are inversely proportional to the NME squared, are given in the last column. Here, the phase-space factor is taken from [68], except for the SM (GCN50.82) [31].

The NME, $M^{(0\nu)}$, in the SM (optimized) is smallest among the various nuclear models in table 2. In particular the GT-type NME of 0.720 is less than half the NME of 1.66 in the SM (SVD) [35]. On the other hand, the absolute value 0.886 of the Fermi-type NME in the SM (optimized) is twice larger than the value of 0.44 in the SM (SVD). The Fermi-type NME becomes much larger in the SM ($1.3G_0$). The cause of the large absolute values of the Fermi-type NME might be a lack of isoscalar effective interactions in the present SM calculations. It was suggested in the QRPA calculations [41] that the NME decreases as the isoscalar pairing strength is made stronger. However, the isoscalar pairing interaction is not taken into account in this paper.

In order to investigate how the NME depends on the wavefunctions of the ground states, the pair-truncated shell-model (PTSM) calculations are also carried out. In the PTSM, the *SD* subspace consisting only of the *S* and *D* pairs, the *SDG* subspace including the *G* pair, and the *SDGH* subspace introduced in the previous section are constructed. Subsequently, the same Hamiltonian as the SM (optimized) is diagonalized within each subspace. The NMEs of the $0\nu\beta\beta$ decay in the PTSM are shown in table 2. It is found that the NMEs in the PTSM gradually approach the SM results as the shell-model subspace increases from the *SD* to the *SDG* and the *SDGH* subspaces. In section 4, much detailed discussions are given.

The NME of the $0\nu\beta\beta$ decay from ^{136}Xe to ^{136}Ba is also calculated in the SM and in the PTSM. The results are shown in table 3. They are compared with the results in other studies, which are previously cited in table 2. It is noted also for ^{136}Xe that the NME in the SM (optimized) is smaller than any other calculations in the SM [31, 35], the GCM [60], the QRPA [47], and the IBM [54].

4. Discussion

In this section, the sensitivity of the NMEs to the wavefunctions in the ground states is investigated further.

First, we calculate the occupation number v_j^2 of the number operator for each orbital j of the ground state, which can be given as

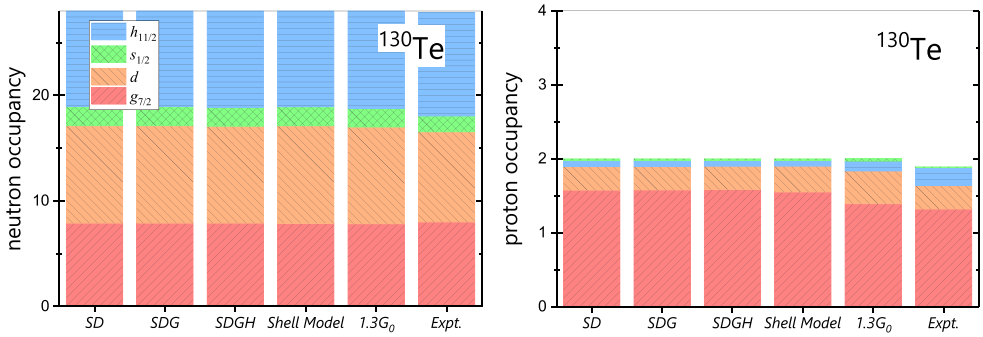

Figure 5. Occupation numbers of ^{130}Te in the several models for neutrons (left panel) and for protons (right panel). In each panel, the numerical results in the PTSM containing *SD*, *SDG*, and *SDGH* pairs are shown on the left three columns, respectively. Those in the SM with the optimized interaction strengths (Shell Model) and those with the 1.3 times stronger monopole pairings ($1.3G_0$) are shown. Experiment data [71, 72] is shown on the far right column of each panel. The symbol of d indicates both the $d_{5/2}$ and $d_{3/2}$ orbitals.

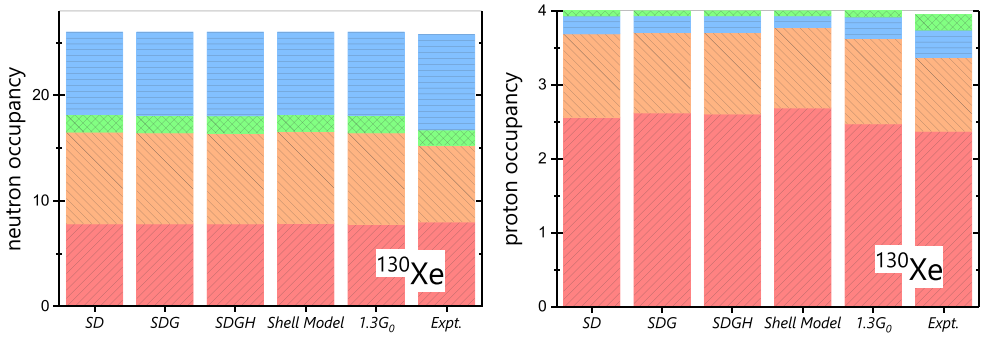

Figure 6. Same as figure 5, but for ^{130}Xe. The experimental data is taken from [71, 72].

$$v_j^2 \equiv \langle \Psi(0^+_{\text{g.s.}})|\ \hat{n}_j|\Psi(0^+_{\text{g.s.}})\rangle, \tag{16}$$

where $\hat{n}_j$ is the number operator of the orbital j and $|\Psi(0^+_{\text{g.s.}})\rangle$ indicates the ground state of a specific nucleus. Figure 5 shows the numerical results of ^{130}Te. The numerical results even match with the experimental data for the strong monopole-pairing (MP) strengths ($1.3G_0$) and for largely reduced model spaces such as the *SD* subspace. This fact indicates that the occupation numbers are insensitive to the nuclear structure or the correlations of the ground-state wavefunctions. As seen in tables 2 and 3, the NMEs change considerably according to the MP strength and the variety of the subspaces in the PTSM. Considering those results, the theoretical realization of the occupation numbers is not directly correlated to the NME. In other words, calculations of the NME in several nuclear models are not always supported even if the occupation numbers are reproduced well.

Figures 6–8 show the occupation numbers in ^{130}Xe, ^{136}Xe, and ^{136}Ba, respectively. We cannot find any significant differences in the occupation numbers among any nuclear models. Those results repeatedly indicate that the occupation numbers have little correlations with the NMEs and the reproduction of the occupation numbers does not necessarily mean that those wavefunctions will provide the correct NMEs. In the present study the NMEs increase

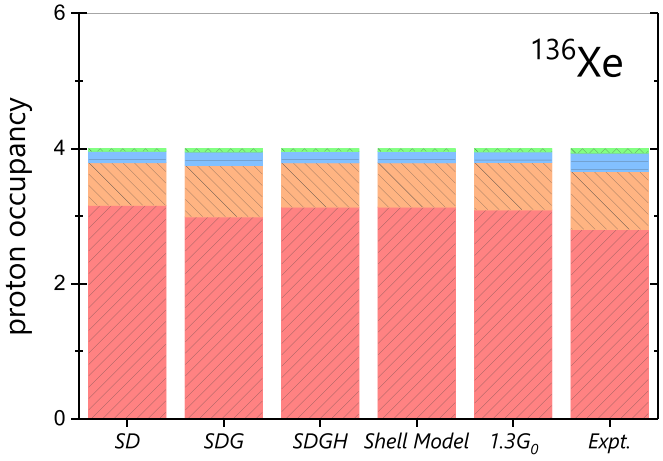

Figure 7. Same as figure 5, but for ^{136}Xe. The experimental data is taken from [72].

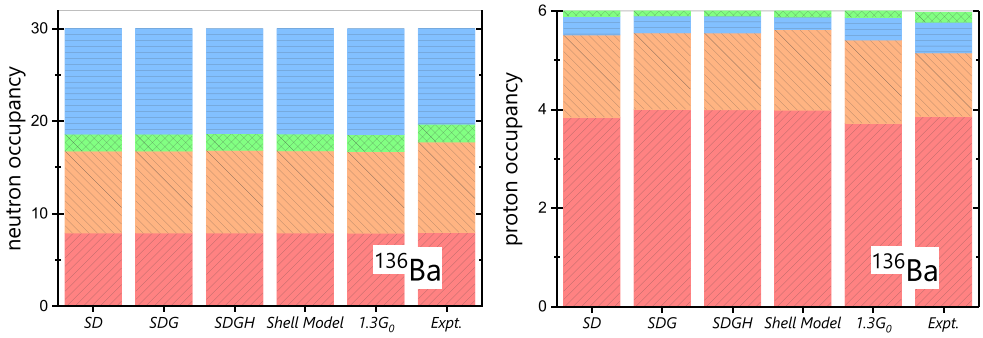

Figure 8. Same as figure 5, but for ^{136}Ba. The experimental data is taken from [72, 73].

monotonically as the shell-model subspace increases from the *SD* to the *SDG* and the *SDGH* subspaces, even though there are less differences concerning the occupancies in valence orbitals. This fact indicates that the occupancies have little influence on the NMEs.

The relevance between the occupancies in valence orbitals and the NMEs has been already discussed in some previous studies. In [74], the values of vacancies were investigated for ^{76}Ge and ^{76}Se. The disagreement in neutron occupancy between QRPA and experiment was reported. However, it was not clear whether the disagreement was relevant on the matrix element for $0\nu\beta\beta$ decay. In [60], it was reported that for ^{124}Sn, ^{124}Te and ^{136}Ba, the occupancies obtained with their GCM calculations were close to the values calculated by the SM. Still the deferences between the NMEs of the GCM and the SM are not negligible. In [75], it was reported that for ^{76}Ge, ^{82}Se, ^{128}Te, ^{130}Te and ^{136}Xe only in some cases the orbital occupancies play a decisive role for the size of the NME, whereas the inclusion of all the spin–orbit partners is essential to achieve a NME of reasonable quality.

In our calculation the overall agreement with the experimental data for the various results is good and there are fewer differences among the number occupancies in the various models. This fact indicates that the single-particle number occupancy does not depend sensitively on the precise structure or correlations of the ground-state wavefunctions. As seen in tables 2 and

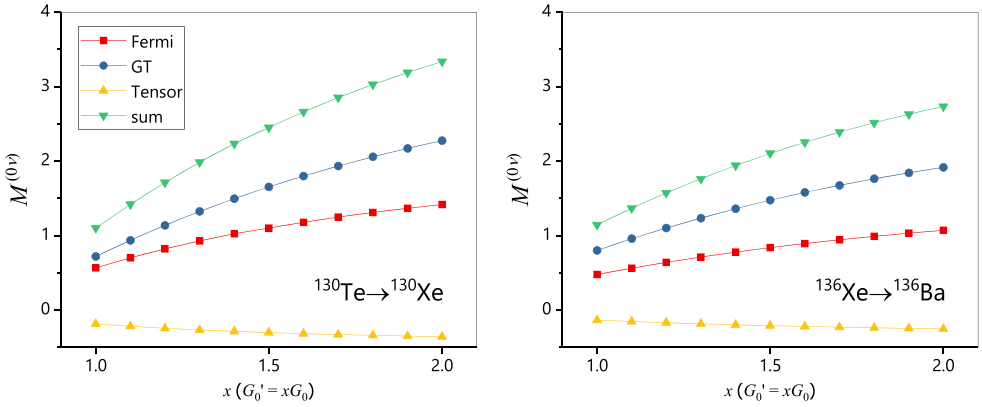

Figure 9. The dependence of NMEs on the pairing-interaction strengths for ^{130}Te to ^{130}Xe decay (left panel), and for ^{136}Xe to ^{136}Ba decay (right panel). The Fermi (Fermi), Gamow–Teller (GT) and Tensor (Tensor) NME components are given as functions of x ($1 \leqslant x \leqslant 2$). The sum (sum) indicates the sum of all the contributions.

3, the NMEs in the various models change considerably according to the different models. This suggests that theoretical realization of the experimental number occupancies is not directly correlated to the NMEs. In other words, calculations of NMEs are not always supported even if the experimental occupancies are reproduced by the ground-state correlations. In this work we find no correlation between the occupation number and the NME and indeed find that the occupation number is insensitive to the calculation. This problem should be further pursued.

Figure 9 shows the dependence of the NMEs on the MP strengths in the shell model (SM). The MP strengths $G_{0\tau}'$ are artificially changed as $G_{0\tau}' = x\ G_{0\tau}$ ($1 \leqslant x \leqslant 2$), where $G_{0\tau}$ indicates the optimized values ($x = 1$). It is found that the NMEs are remarkably increased as the MP strengths are larger. If the MP strengths are 1.3 times larger than the optimized values, the NMEs become 1.8 times (1.5 times) larger for ^{130}Te to ^{130}Xe decay (for ^{136}Xe to ^{136}Ba decay). In fact the NMEs with $x = 1.3$ already exceed the results in the other SM calculations, and those with $x = 2$ exceed the results in the other models except the IBM.

The NMEs can be decomposed with the angular momentum J of two decaying neutrons as

$$M_K^{(0\nu)}(J) = \langle \Psi_{\rm fin}(0^+_{\rm g.s.})|\ \hat{V}_K^{(J)} |\Psi_{\rm ini}(0^+_{\rm g.s.})\rangle, \tag{17}$$

where $\hat{V}_K^{(J)}$ is the neutrino potential $\hat{V}_K$ decomposed with the coupled pair angular momentum J as

$$\hat{V}_K = \sum_J \hat{V}_K^{(J)} \tag{18}$$

with

$$\hat{V}_K^{(J)} = \sum_{j_1 j_2 j_3 j_4} V^{(\lambda)}_{s_1,s_2}(j_1 j_2 j_3 j_4;\, J)([c^\dagger_{\pi j_1}\, c^\dagger_{\pi j_2}]^{(J)} \cdot [\tilde{c}_{\nu j_3} \tilde{c}_{\nu j_4}]^{(J)}). \tag{19}$$

The two-body matrix elements $V^{(\lambda)}_{s_1,s_2}(j_1 j_2 j_3 j_4\,;\, J)$ are given in [39, 51]. Our results shown in figure 10 are consistent with another SM study [30], where the $J = 0$ components give the largest contributions and the second largest contributions arise from the $J = 2$ components.

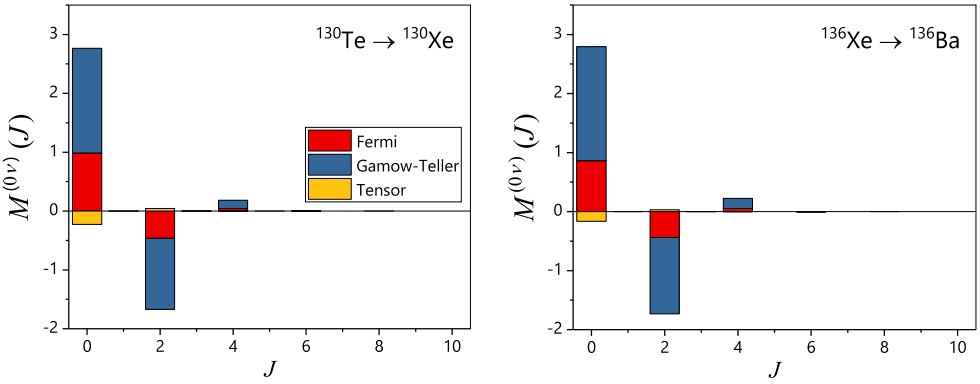

Figure 10. Contributions to the NME from spin J pair for ^{130}Te to ^{130}Xe decay (left panel), and for ^{136}Xe to ^{136}Ba decay (right panel).

Table 4. Upper limits (last column) for the effective neutrino mass in unit of eV using the ^{130}Te theoretical half life $T^{(0\nu)}_{1/2}$ times the effective neutrino mass $\langle m_\nu \rangle$ (second column) in units of 10^{25} yr $\cdot$ eV^2.

Models	$M^{(0\nu)}$	$T^{(0\nu)}_{1/2}\langle m_\nu \rangle^2$	$\langle m_\nu \rangle$
SM (optimized)	1.101	0.618	$\leqslant$0.64
SM (1.3G_0)	1.986	0.190	$\leqslant$0.31
PTSM (*SD*)	2.631	0.108	$\leqslant$0.27
ISM (Jastrow) [31]	2.12	0.129	$\leqslant$0.29
IBM [54]	3.70	0.052	$\leqslant$0.19

Table 5. Same as table 5, but for ^{136}Xe decay.

Models	$M^{(0\nu)}$	$T^{(0\nu)}_{1/2}\langle m_\nu \rangle^2$	$\langle m_\nu \rangle$
SM (optimized)	1.145	0.557	$\leqslant$0.228
SM (1.3G_0)	1.763	0.235	$\leqslant$0.148
PTSM (*SD*)	1.787	0.229	$\leqslant$0.146
ISM (Jastrow) [31]	1.76	0.178	$\leqslant$0.129
IBM [54]	3.05	0.074	$\leqslant$0.083

The sensitivity of the NMEs on the MP strengths as shown in figure 9 can be understood from the fact that the $J = 0$ contributions are enhanced by the strong MP strengths.

Recently, experimental results [76] for the cosmic microwave background provided the upper limit on the effective neutrino mass that $\langle m_\nu \rangle \leqslant 0.12$ eV. In contrast, lower limits on the $0\nu\beta\beta$ decay half-life of ^{136}Xe [61, 62] and that of ^{130}Te [63] have been reported. The lower limits are 1.07×10^{26} yr for ^{136}Xe and 1.5×10^{25} yr for ^{130}Te so far. Using the results of the precise experiments and the NMEs calculated in the various nuclear models, the upper limits on the effective neutrino mass are given in tables 4 and 5. The upper limits in the SM with the optimized interactions are consistent with the experimental results [76], whereas the IBM result for ^{136}Xe gives the stronger constraint for the effective neutrino mass.

5. Summary and conclusions

In the present study, nuclear shell-model (SM) calculations are carried out for the ^{130}Te, ^{130}Xe, ^{136}Xe, and ^{136}Ba nuclei. The NMEs of the neutrinoless double beta ($0\nu\beta\beta$) decays from ^{130}Te to ^{130}Xe and from ^{136}Xe to ^{136}Ba are calculated with the use of the wavefunctions of the ground states in the SM. Comparing our results with other SM studies, the quasi-particle random phase approximation (QRPA), the interacting boson model (IBM), and the GCM, the NMEs in the present SM study are found to be considerably smaller.

In order to investigate the dependence of the NMEs on the wavefunctions, the SM calculations with the isovector monopole-pairing (MP) strengths which are artificially made larger than the optimized values are also performed. It is found that the NMEs have strong correlations on the MP strengths since the NMEs monotonically increase as the MP strengths are larger. In addition, the PTSM is applied for the evaluation of the NME where the SM space is truncated to the subspace consisting of collective pairs and a non-collective pair associated with the $0h_{11/2}$ orbital. It is shown that by expanding the model space in the PTSM from *SD* to *SDG* and *SDGH* subspaces, the NMEs gradually approach the SM results. Those results suggest that the ground-state correlations are important for the NMEs of the neutrinoless double beta decay.

The occupation number of the number operator for each orbital j has been calculated in the ground states. The experimental results are reproduced well in the SM and there are little differences among the various models such as the SM with the 1.3 times stronger MP strengths and the PTSM. This fact indicates that the occupation number does not depend sensitively on the precise structure or correlations of the ground-state wavefunctions. In other words calculations of NMEs are not always supported even if the experimental occupancies are reproduced by the ground-state wavefunctions.

In the present approach the sensitivity of the NMEs to the isovector MP strengths is investigated. However, it was reported in recent papers [60, 77] that the isoscalar MP strengths play an important role in predicting the NME of the $0\nu\beta\beta$ decay. We have not treated the isoscalar pairing interactions in this study because of the lack of our formulation in the SM code. In our future work we will consider effects of these interactions on the NMEs by expanding our formulation.

Acknowledgments

This work was supported by Grant-in-Aid for Scientific Research (C) (Nos. 16K05341 and 17K05450) from the Japan Society for the Promotion of Science (JSPS).

ORCID iDs

K Higashiyama https://orcid.org/0000-0002-0310-7757

References

[1] Koike T, Starosta K, Chiara C J, Fossan D B and LaFosse D R 2001 *Phys. Rev.* C **63** 061304(R)
[2] Kuti I *et al* 2013 *Phys. Rev.* C **87** 044323
[3] Hartley D J *et al* 2001 *Phys. Rev.* C **64** 031304(R)
[4] Budaca R 2018 *Phys. Rev.* C **98** 014303
[5] Bhat G H, Sheikh J A and Palit R 2012 *Phys. Lett.* B **707** 250–4

[6] Shimada M, Fujioka Y, Tagami S and Shimizu Y R 2018 *Phys. Rev.* C **97** 024319
[7] Yoshinaga N and Higashiyama K 2006 *Eur. Phys. J.* A **30** 343–6
[8] Higashiyama K and Yoshinaga N 2007 *Eur. Phys. J.* A **33** 355–74
[9] Higashiyama K and Yoshinaga N 2008 *Prog. Theor. Phys.* **120** 525–48
[10] Yoshinaga N, Higashiyama K and Arai R 2010 *Prog. Theor. Phys.* **124** 1115–23
[11] Higashiyama K and Yoshinaga N 2005 *Prog. Theor. Phys.* **113** 1139–44
[12] Higashiyama K, Yoshinaga N and Tanabe K 2005 *Phys. Rev.* C **72** 024315
[13] Yoshinaga N and Higashiyama K 2005 *J. Phys. G: Nucl. Part. Phys.* **31** S1455
[14] Higashiyama K and Yoshinaga N 2013 *Phys. Rev.* C **88** 034315
[15] Valiente-Dobón J J *et al* 2004 *Phys. Rev.* C **69** 024316
[16] Leguillon R *et al* 2013 *Phys. Rev.* C **88** 044309
[17] Nishibata H *et al* 2015 *Phys. Rev.* C **91** 054305
[18] Teruya E, Yoshinaga N, Higashiyama K and Odahara A 2015 *Phys. Rev.* C **92** 034320
[19] Teruya E, Yoshinaga N, Higashiyama K, Nishibata H, Odahara A and Shimoda T 2016 *Phys. Rev.* C **94** 014317
[20] Avignone F T, Elliott S R and Engel J 2008 *Rev. Mod. Phys.* **80** 481–516
[21] Fukugita M and Yanagida T 2013 *Physics of Neutrinos: and Application to Astrophysics* (Berlin: Springer Science & Business Media)
[22] Barabash A S 2010 *Nucl. Phys.* A **935** 52–64
[23] Tomoda T 1991 *Rep. Prog. Phys.* **54** 53
[24] Nakada H, Sebe T and Muto K 1996 *Nucl. Phys.* A **607** 235–49
[25] Štefánik D, Šimkovic F, Muto K and Faessler A 2013 *Phys. Rev.* C **88** 025503
[26] Yoshida N and Iachello F 2013 *Prog.Theor. Exp. Phys.* **2013** 043D01
[27] Coraggio L, De Angelis L, Fukui T, Gargano A and Itaco N 2017 *Phys. Rev.* C **95** 064324
[28] Cremonesi O and Pavan M 2014 *Adv. High Energy Phys.* **2014** 951432
[29] Haxton W and Stephenson G Jr 1984 *Prog. Part. Nucl. Phys.* **12** 409–79
[30] Caurier E, Menéndez J, Nowacki F and Poves A 2008 *Phys. Rev. Lett.* **100** 052503
[31] Menéndez J, Poves A, Caurier E and Nowacki F 2009 *Nucl. Phys.* A **818** 139–51
[32] Horoi M and Stoica S 2010 *Phys. Rev.* C **81** 024321
[33] Horoi M 2013 *Phys. Rev.* C **87** 014320
[34] Horoi M and Brown B A 2013 *Phys. Rev. Lett.* **110** 222502
[35] Neacsu A and Horoi M 2015 *Phys. Rev.* C **91** 024309
[36] Horoi M and Neacsu A 2016 *Phys. Rev.* C **93** 024308
[37] Iwata Y, Shimizu N, Otsuka T, Utsuno Y, Menéndez J, Honma M and Abe T 2016 *Phys. Rev. Lett.* **116** 112502
[38] Sen'kov R A and Horoi M 2016 *Phys. Rev.* C **93** 044334
[39] Yoshinaga N, Yanase K, Higashiyama K, Teruya E and Taguchi D 2018 *Prog. Theor. Exp. Phys.* **2018** 023D02
[40] Šimkovic F, Pantis G, Vergados J D and Faessler A 1999 *Phys. Rev.* C **60** 055502
[41] Rodin V A, Faessler A, Šimkovic F and Vogel P 2003 *Phys. Rev.* C **68** 044302
[42] Kortelainen M, Civitarese O, Suhonen J and Toivanen J 2007 *Phys. Lett.* B **647** 128–32
[43] Kortelainen M and Suhonen J 2007 *Phys. Rev.* C **75** 051303(R)
[44] Šimkovic F, Faessler A, Müther H, Rodin V and Stauf M 2009 *Phys. Rev.* C **79** 055501
[45] Šimkovic F, Faessler A and Vogel P 2009 *Phys. Rev.* C **79** 015502
[46] Mustonen M T and Engel J 2013 *Phys. Rev.* C **87** 064302
[47] Šimkovic F, Rodin V, Faessler A and Vogel P 2013 *Phys. Rev.* C **87** 045501
[48] Faessler A, González M, Kovalenko S and Šimkovic F 2014 *Phys. Rev.* D **90** 096010
[49] Hyvärinen J and Suhonen J 2015 *Phys. Rev.* C **91** 024613
[50] Fang D L, Faessler A and Šimkovic F 2018 *Phys. Rev.* C **97** 045503
[51] Barea J and Iachello F 2009 *Phys. Rev.* C **79** 044301
[52] Barea J, Kotila J and Iachello F 2012 *Phys. Rev. Lett.* **109** 042501
[53] Barea J, Kotila J and Iachello F 2013 *Phys. Rev.* C **87** 014315
[54] Barea J, Kotila J and Iachello F 2015 *Phys. Rev.* C **91** 034304
[55] Rodríguez T R and Martínez-Pinedo G 2013 *Phys. Lett.* B **719** 174–8
[56] Vaquero N L, Rodríguez T R and Egido J L 2013 *Phys. Rev. Lett.* **111** 142501
[57] Yao J M, Song L S, Hagino K, Ring P and Meng J 2015 *Phys. Rev.* C **91** 024316
[58] Yao J M and Engel J 2016 *Phys. Rev.* C **94** 014306
[59] Hinohara N and Engel J 2014 *Phys. Rev.* C **90** 031301(R)

[60] Jiao C F, Horoi M and Neacsu A 2018 *Phys. Rev.* C **98** 064324
[61] Gando A *et al* (KamLAND-Zen Collaboration) 2016 *Phys. Rev. Lett.* **117** 082503
[62] Albert J B *et al* (EXO-200 Collaboration) 2018 *Phys. Rev. Lett.* **120** 072701
[63] Alduino C *et al* (CUORE Collaboration) 2018 *Phys. Rev. Lett.* **120** 132501
[64] Singh B 2001 *Nucl. Data Sheets* **93** 33–242
[65] Astier A *et al* 2014 *Eur. Phys. J.* A **50** 2
[66] Mccutchan E A 2018 *Nucl. Data Sheets* **152** 331–667
[67] Vergados J D, Ejiri H and Šimkovic F 2012 *Rep. Prog. Phys.* **75** 106301
[68] Kotila J and Iachello F 2012 *Phys. Rev.* C **85** 034316
[69] Kotila J and Iachello F 2013 *Phys. Rev.* C **87** 024313
[70] Miller G A and Spencer J E 1976 *Ann. Phys.* **100** 562–606
[71] Kay B P *et al* 2013 *Phys. Rev.* C **87** 011302
[72] Entwisle J P *et al* 2016 *Phys. Rev.* C **93** 064312
[73] Szwec S V *et al* 2016 *Phys. Rev.* C **94** 054314
[74] Schiffer J P *et al* 2008 *Phys. Rev. Lett.* **100** 112501
[75] Suhonen J and Civitarese O 2010 *Nucl. Phys.* A **847** 207
[76] Aghanim N *et al* 2018 *Planck 2018 results. VI. Cosmological parameters* arXiv:1807.06209
[77] Menéndez J, Hinohara N, Engel J, Martínez-Pinedo G and Rodríguez T R 2016 *Phys. Rev.* C **93** 014305